

DRAFT

Long Term Maritime Aerosol Optical Depth Analysis: Program Description and Results

Ellsworth J. Welton, Kenneth J. Voss, and Joseph M. Prospero

To Be Submitted to the Journal of Geophysical Research: Spring 1997

Abstract: The radiative properties of atmospheric aerosols are an important element of the global radiation balance and in applications such as remote sensing. One of the most important radiative properties is the aerosol optical depth (AOD) and its associated wavelength dependence; characterized by the Angstrom exponent, α . Long term measurements of these aerosol features taken at various locations are necessary to track seasonal patterns of radiative behavior and to determine characteristic differences in the optical properties of different sites. An AOD measurement program was begun in August of 1993 to determine the radiative properties of aerosols over existing Atmosphere/Ocean Chemistry Experiment (AEROCE) sites in Miami, Florida, Bermuda, and Barbados. A description of the radiative program, instrumentation and calibration procedures, the methodology employed to determine the AOD and α , and the final results obtained from the measurements are presented. Analysis of the AOD and Angstrom exponents in terms of seasonal variations and unique site characteristics were performed as well.

Keywords: Aerosols, Optical Depth, Angstrom Exponent, sunphotometer, shadowband

1. INTRODUCTION

There is relatively little information on the climatology of atmospheric aerosols, particularly over the ocean. However, the radiative effects of marine aerosols directly alter terrestrial optical properties, such as the planetary albedo, and may play an important role, directly and indirectly, in the global climate [Charlson, 1992]. In addition to the terrestrial impact of marine aerosols they also affect our ability to extract surface information from satellites, in particular for ocean color remote sensing [Gordon, ???]. Knowledge of the aerosol optical properties are necessary to correct for these effects in both Global Circulation Models and in satellite correction algorithms.

The most commonly measured aerosol optical property is the aerosol optical depth (AOD), which determines how the aerosol attenuates the direct solar beam. The total optical depth, $\tau(\lambda)$, is defined by

$$\tau(\lambda) = \frac{1}{m(\vartheta_z)} \text{Ln} \left[\frac{E_o(\lambda)}{E(\lambda)} \right], \quad (1)$$

where $m(\vartheta_z)$ is the air mass at zenith angle ϑ_z , $E_o(\lambda)$ is the extra-terrestrial solar irradiance (solar constant) at wavelength λ , and $E(\lambda)$ is the direct, unscattered solar irradiance at the surface. For wavelengths that lie outside the usual atmospheric gas absorption bands, the total optical depth may also be written as the sum

$$\tau(\lambda) = \tau_r(\lambda) + \tau_o(\lambda) + \tau_w(\lambda) + \tau_a(\lambda) \quad (2)$$

where $\tau_r(\lambda)$ is the Rayleigh optical depth due to molecular scattering, $\tau_o(\lambda)$ is the Chappius band ozone optical depth, $\tau_w(\lambda)$ is the optical depth due to water vapor absorption, and $\tau_a(\lambda)$ is

the aerosol optical depth. The basic experimental method of acquiring the AOD from the total optical depth has been outlined in several papers, most notably *Shaw* [1979] and *King et al.* [1980].

The spectral variation of the AOD can be used to extract additional useful information on the aerosols. One convenient spectral parameterization uses the fact that the AOD is often proportional to some power of the wavelength [*Angstrom* , 1964], and is written as

$$\tau_a(\lambda) = \beta \lambda^{-\alpha} , \quad (3)$$

where λ is the wavelength, α is the Angstrom exponent, and β is a scale factor. In the special case of a Junge type size distribution ($dn/dr = Cr^{-(r+1)}$), the Angstrom exponent is related to the slope of the size distribution of the aerosol scatterers [*Van de Hulst*, 1981]. The exponent, α , generally varies from zero to two, with lower exponents representing a lower ratio of small to larger sized particles than in the case with a higher exponent.

Greenhouse gases are typically long-lived and diffuse, and while they are important, their effects can be modeled. Aerosols, by contrast, have short lifetimes and are highly inhomogeneous and variable. To determine the possible radiative impact of aerosols, long term studies of the optical properties of the aerosols at many locations are required. As one of our objectives is to determine the optical climatology of the aerosols over the ocean, these measurements can be performed from ships or small islands. Island locations are convenient for multi-year observational records as local observers can be used and logistical problems are reduced.

In order to obtain long term data sets of the AOD and other physical aerosol measurements, hand-held sunphotometers were used at existing AEROCE (Atmosphere/Ocean Chemistry Experiment) sites in Miami (Florida), Bermuda, and Barbados. Utilization of the AEROCE stations [*Reference ???*] for the sunphotometer measurements was advantageous because problems associated with operating long term remote sites in foreign countries were reduced. In addition,

these sites perform a variety of measurements of the chemical and physical properties of the boundary layer aerosols. The hand-held sunphotometers were replaced with Automated Multi-Filter Rotating Shadowband Radiometers [Harrison *et al.*, 1994] by the end of 1994. The shadowbands create a more complete data record as they automatically sample all day, perform a potential calibration each day (dependent on weather), and also measure diffuse irradiance. The shadowbands operated concurrently with the sunphotometers for several months during the instrument replacement process. Table 1 indicates the geographical information and time period of the sunphotometer and shadowband measurements at each site. The instrument calibration procedure, methods of data selection, aerosol optical depths, and Angstrom exponents recorded for each site are presented in this paper.

2. INSTRUMENT PROGRAM DESCRIPTION AND CALIBRATION

The sunphotometers used to generate the AOD data sets in Miami, Bermuda, and Barbados each had nine channels containing an interference filter. New filters were installed in each instrument at the beginning of the measurement period reported in the paper. Identical filters, selected from the same lot, were used in all the sunphotometers. The spectral bandwidth of each sunphotometer channel filter had a passband approximately 5 nm wide centered at wavelengths from 380.2 to 1025.9 nm (Table 2). Each shadowband had seven channels containing an interference filter, except for channel one which was a broadband channel (no spectral filter). The spectral bandwidth of shadowband filters two through seven are 10 nm wide, and are centered at wavelengths from 410 to 940 nm (Table 2). Channel seven of the shadowbands is located in a water vapor absorption band in order to obtain $\tau_w(\lambda)$. Neither water vapor analysis or broadband studies were a focus of this project, therefore data from shadowband channels one and seven was not used. The remaining filter wavelengths in each instrument were chosen to avoid strong absorption bands such as water vapor, thus simplifying equation 2 as $\tau_w(\lambda)$ was taken to be zero.

However, avoidance of the ozone Chappius band was not possible, therefore ozone absorption must be taken into account in the data reduction process.

The sunphotometers were operated by on site personnel who recorded measurements at approximately 10:00 am and 3:00 pm local time respectively. The shadowbands ran automatically, eliminating the need for an on site operator, however, on site personnel are needed in the event of instrument malfunction or equipment upgrades. The Miami shadowband sampled data every minute throughout the day, while the Bermuda and Barbados shadowbands sampled every four minutes to reduce the number of data downloads per week. As the shadowbands perform measurements continually, each day offers the potential of a Langley calibration [Shaw, 1983]. Therefore the calibrations for the shadowbands are more complete than those for the sunphotometers.

A calibration record (history) for each instrument was compiled in order to account for time shifts in the solar constants of each channel, often caused by degradation of the filter. The calibration record for an instrument refers to the plot of the date versus $E_o(\lambda)$ for the length of the entire data set. A fit to this plot allows the solar constants, on a day that did not allow a Langley calibration to be performed, to be calculated using the fitted equation. An error correction procedure was then employed for both instruments to modify the conventional Langley calibration. The sunphotometer and shadowband calibration procedures are outlined below.

2a. SUNPHOTOMETER DATA PROGRAM AND CALIBRATION

A sunphotometer was located at each site, while an additional sunphotometer was used for calibration processes during and after the measurement period. Initially the Langley method was used to perform the calibrations, for each sunphotometer, in Miami prior to deployment into the field. The instruments were then sent into the field, and operations began as indicated in Table 1. With the exception of poor weather days, the measurements continued uninterrupted for the

remainder of the sunphotometer program. Sea level Langley calibrations in these locations are difficult due to atmospheric instability and cloudiness. Thus it was not possible to perform routine Langley calibrations at the Bermuda and Barbados locations. The Miami instrument (M114) was calibrated several times during the sunphotometer program, both in Miami and in Brainard Lake, Colorado. An additional sunphotometer (M119), not tied to any location, was extensively calibrated during an oceanographic cruise, off of Hawaii, in October and November of 1994. Post-calibrations for the Bermuda and Barbados instruments were performed in Miami at the end of the sunphotometer program (through a method described below). Calibration values were obtained for days within the data set using an interpolation between the initial calibrations and the post-calibrations. Prior experience with the sunphotometer interference filters led us to use an exponential function to fit the decay of these filters for the interpolation.

It was difficult to perform full Langley calibrations on the instruments at the end of the sunphotometer program due to poor weather. The Miami instrument was calibrated several times during the initial startup, and throughout the program, and was considered to be the best calibrated of the sunphotometers. The M119 sunphotometer was well calibrated, using the Langley procedure, during October and November 1994 and was used to calibrate the Miami instrument at the end of the sunphotometer program through a cross-calibration procedure. A cross-calibration assumes that two identical sunphotometers are present, one is fully calibrated and is referred to as the reference instrument, the other is uncalibrated and referred to as the target instrument. Simultaneous direct beam measurements are made with each sunphotometer at the same location. The resulting equations for each instrument are

$$E_r(\lambda) = E_{r_0}(\lambda) \exp[-\tau(\lambda)m_r(\vartheta_z)], \quad (4)$$

$$E_t(\lambda) = E_{t_0}(\lambda) \exp[-\tau(\lambda)m_t(\vartheta_z)], \quad (5)$$

where the r subscript denotes the reference instrument, the t subscript denotes the target instrument, and $m(\vartheta_z)$ is the air mass at zenith angle, ϑ_z , computed using the formula provided by *Kasten and Young* [1989]. $E_r(\lambda)$ and $E_t(\lambda)$ are the measured direct solar irradiances in instrument counts, and $E_{r_o}(\lambda)$ and $E_{t_o}(\lambda)$ are the extraterrestrial solar irradiances in instrument counts for the reference and target instruments. As $E_{r_o}(\lambda)$ is known, the total optical depth is calculated using the calibrated instrument. Once the total optical depth is determined, $E_{t_o}(\lambda)$, can be written as

$$E_{t_o}(\lambda) = E_{r_o}(\lambda) \frac{E_t(\lambda)}{E_r(\lambda)} \exp[\tau(\lambda)(m_t(\vartheta_z) - m_r(\vartheta_z))], \quad (6)$$

for each wavelength of the sunphotometer. This cross-calibration procedure was useful as the weather need only be stable and cloud free for a small window of time, as opposed to the requirements for a Langley calibration. The total optical depth changes for different air masses, therefore the two values, $m_r(\vartheta_z)$ and $m_t(\vartheta_z)$, should be as close as possible to avoid errors in calculating $E_{t_o}(\lambda)$. If the measurements are made close to solar noon, the air mass changes very little during the measurement process and the exponential term is negligible. This procedure also assumes that the instruments have matched wavelengths ($\lambda_r = \lambda_t$), and in our case the filters were matched for all sunphotometers.

Once the Miami instrument, (M114), had been cross-calibrated against M119, the cross-calibrations were added to the calibration history for M114, and it was considered fully calibrated. M114 was then used as a reference instrument during cross-calibrations for the Bermuda and Barbados sunphotometers. These cross-calibrations were then added to the calibration history for

Bermuda and Barbados. The calibration histories for the three locations are given in Figs. 1a, 1b, and 1c. The solid line is the exponential fit to the calibrations given above.

An error correction procedure was utilized to fine tune these solar constants. This procedure assumes that there is some error, $\chi(\lambda)$, present in the solar constant, and that the aerosols above the sites, on average, obey the Angstrom spectral dependence (Eq. (3)). Redefining the solar constant in terms of this error and the true solar constant yields

$$E_o(\lambda) = \chi(\lambda)E'_o(\lambda), \quad (7)$$

where $E_o(\lambda)$ is the previously derived solar constant, $\chi(\lambda)$ is the error factor, and $E'_o(\lambda)$ is the true solar constant. The measured total optical depth is given by

$$\tau(\lambda) = \frac{1}{m(\vartheta_z)} \text{Ln} \left[\frac{E_o(\lambda)}{E(\lambda)} \right] = \frac{1}{m(\vartheta_z)} \text{Ln} \left[\frac{E'_o(\lambda)}{E(\lambda)} \right] + \frac{\text{Ln}[\chi(\lambda)]}{m(\vartheta_z)}, \quad (8)$$

using Eq. (7). The true optical depth would be

$$\tau'(\lambda) = \frac{1}{m(\vartheta_z)} \text{Ln} \left[\frac{E'_o(\lambda)}{E(\lambda)} \right] \quad (9)$$

as follows from Eq. (1). Using Eqs. (8) and (9) the following equation can be calculated

$$\text{Ln}[\chi(\lambda)] = [\tau(\lambda) - \tau'(\lambda)]m(\vartheta_z) \quad (10)$$

relating the error factor $\chi(\lambda)$, to the difference in measured and true total optical depths. The calculated Rayleigh optical depth [Hansen *et al.*, 1974] and the ozone optical depth, computed using ozone profiles provided by Klenk *et al.* [1983], are subtracted from both the measured and true total optical depths. The resulting equation

$$\text{Ln}[\chi(\lambda)] = [\tau_a(\lambda) - \tau'_a(\lambda)]m(\vartheta_z), \quad (11)$$

relates the error factor, $\chi(\lambda)$, to the difference in measured and true aerosol optical depths.

During the calibration process, a sunphotometer reading consisted of recording $E(\lambda)$ for each of the nine wavelengths. The AOD derived from $E(\lambda)$, using $E_o(\lambda)$, was then fit to Eq. (3), determining β and α , and this equation was then used to generate $\tau'_a(\lambda)$ producing the final relation

$$\text{Ln}[\chi(\lambda)] = [\tau_a(\lambda) - \beta\lambda^{-\alpha}]m(\vartheta_z). \quad (12)$$

Therefore, $\text{Ln}[\chi(\lambda)]$, is the difference between the measured AOD and the Angstrom fitted AOD for a given wavelength, times the air mass. This factor determines the variation from the Angstrom power law for that particular measurement.

The AOD, for each location's entire data set, was first calculated using the original solar constants, and the Rayleigh and ozone models cited above. For each day, the deviation of the AOD from the Angstrom power law was determined and used to generate the error factor $\chi(\lambda)$. The error factors calculated during the sunphotometer program were fit by another exponential function, yielding an equation for $\chi(\lambda)$ for each instrument. The resulting error factors were used to correct the solar constants according to Eq. (7). The error-corrected solar constant histories are

plotted in Figs. 1a, 1b, and 1c as the dotted lines. Channels one (380.2 nm) and nine (1025.9 nm) were not processed, and were not used in this paper. The 380.2 nm filter degraded rapidly in all instruments and was considered unusable. Channel nine deviated significantly from the Angstrom power law, perhaps due to the weak water vapor absorption band around 1000 nm [Shaw, 1979] which was not considered in our analysis, or the effects of sea spray [Villevaude *et. al.*, 1994]. These error corrected calibration values are not significantly different from the original values but provide a fine tuning adjustment.

2b. SHADOWBAND DATA PROGRAM AND CALIBRATION

The shadowbands began operation in the fall of 1994. The time periods of the shadowband program are indicated in Table 1. Gaps are present in all data sets due to instrument malfunctions and the subsequent time needed to repair the problems. A gap exists in the Miami data from September 1995 to November 1995. This was caused by data communication problems and poor weather. Normal operation began again in December 1995. The Bermuda data gap, also caused by data communication problems, resulted in the loss of data from July 1995 to November 1995. The communication problems were fixed in December 1995 and shadowband operation was continued. The Barbados shadowband data set only includes data from May 1995 to August 1995 due to poor phone line connections for data transfer and unstable electrical power at the site. These problems have been fixed by new phone line connections to the site and the installation of an uninterruptable power supply (UPS) for the shadowband. Barbados shadowband operation began again after the end of 1995.

All of the shadowbands collect enough data each day to perform two Langley calibrations, one in the morning and one in the afternoon, weather permitting. Therefore all that remains is to determine which of the days has weather suitable for Langley calibrations. Each shadowband's data set was analyzed using the Objective Langley Regression Algorithm (OLRA) [Harrison and Michalsky, 1994] in order to recover the solar constants for each shadowband. The OLRA rejected

a large number of the Langley calibrations for all three sites due to the variable tropical weather at each location. However, this strict criteria assures that the remaining Langley calibrations are accurate. Once the solar constants for each shadowband were determined using this technique, a calibration history was compiled in the same manner as for the sunphotometers. The calibration histories for each shadowband and interpolations are depicted in Figs. 2a, 2b, and 2c. There were few solar constant values recovered for the Barbados shadowband due to the small time period of the data set. Therefore, the solar constants for the Barbados shadowband were obtained by using the mean value of the solar constant for each channel instead of the interpolations described above.

A linear fit to the calibration histories was performed for all of the channels except channel four (610 nm) of the Miami shadowband, and channels four and five (610 and 665 nm respectively) of the Bermuda shadowband. The filters in these channels were found to stabilize after a period of time making a singular linear fit unsuitable. Instead a linear fit was performed on the first part of the calibrations, ignoring the stabilized portion, and a second linear fit was performed on the stabilized portion.

These Langley calibrations were fine tuned with another procedure. This procedure assumes that there is some error, $\mu(\lambda)$, present in the solar constant, but the assumption that the aerosol above the sites obey the Angstrom spectral dependence on average is not necessary. As more measurement samples are recorded by the shadowband than with the sunphotometer it is possible instead to analyze a month's worth of data to test for dependence of the AOD on solar zenith angle. By definition, the set of minimum aerosol optical depths should not depend on solar zenith angle (air mass), over the span of one month. A plot of the AOD versus $m(\vartheta_z)^{-1}$ for a given month should have the lowest AOD's represent a background AOD. A linear fit to the lowest AOD's in the plot described above should have zero slope and a y intercept equal to the average background AOD for that month. A slope not equal to zero would indicate that the background AOD has some dependence on the air mass that may only have been caused by error in the solar constant, $E_o(\lambda)$, [Reference ???, personal correspondence] as detailed below.

Assuming that there is some error, $\mu(\lambda)$, in the solar constants yields the following equation

$$E_o(\lambda) = \mu(\lambda)E'_o(\lambda), \quad (13)$$

where $E_o(\lambda)$ is the previously derived solar constant, $\mu(\lambda)$ is the error factor, and $E'_o(\lambda)$ is the true solar constant. Inserting Eq. (13) into Eq. (1) produces the following relation

$$\tau(\lambda) = \frac{\text{Ln}[\mu(\lambda)]}{m(\vartheta_z)} + \frac{1}{m(\vartheta_z)} \text{Ln}\left[\frac{E'_o(\lambda)}{E(\lambda)}\right] = \frac{\text{Ln}[\mu(\lambda)]}{m(\vartheta_z)} + \tau'(\lambda), \quad (14)$$

$\tau'(\lambda)$ is the true optical depth as it contains the true solar constant, $E'_o(\lambda)$. The Rayleigh and ozone optical depths are not dependent on the calibrations so they may be subtracted from both sides of Eq. (14) to produce the equation

$$\tau_a(\lambda) = \frac{1}{m(\vartheta_z)} \text{Ln}[\mu(\lambda)] + \tau'_a(\lambda). \quad (15)$$

Equation 15 may only be used when both $\tau_a(\lambda)$ and $\tau'_a(\lambda)$ represent the background (minimum) AOD, as other values of $\tau_a(\lambda)$ and $\tau'_a(\lambda)$ may have a dependence on the air mass. Therefore, the slope of the background AOD versus $m(\vartheta_z)^{-1}$ plot described above is the natural logarithm of $\mu(\lambda)$. This procedure may be used to obtain monthly values of $\mu(\lambda)$ for each shadowband channel. The shadowband error corrected solar constants were obtained by first calculating the

solar constant from the linear fit and then using the appropriate month's $\mu(\lambda)$ in Eq. (13). The error corrected solar constants are plotted in Figs. 2a, 2b, and 2c..

3. AOD AND ANGSTROM EXPONENT CALCULATIONS

The final aerosol optical depths and corresponding Angstrom exponents were calculated for Miami, Bermuda, and Barbados using both the sunphotometer and shadowband data. The uncorrected calibration fits and the error corrected calibrations described above were applied to the data sets separately in order to gauge the usefulness of the error correction procedures. Data filtering procedures were then used to remove optical data affected by atmospheric phenomena other than aerosols, such as clouds. Both data filtering procedures were similar, but due to the nature of the instruments, a different filtering procedure was employed for each instrument. The filtering procedures and comparisons between the uncorrected and error corrected results are described below.

3a. SUNPHOTOMETER DATA FILTERING PROCEDURE

The aerosol optical depths and Angstrom exponents were only calculated for channels two to eight, for the respective data sets, due to the calibration problems with channels one and nine. The sunphotometer data filter contained three levels. Level one determined the deviation of the measured $\tau_a(\lambda)$ from the power law fitted $\tau'_a(\lambda)$ for a given measurement, similar to the error factor procedure above. If the magnitude of the deviation between $\tau_a(\lambda)$ and $\tau'_a(\lambda)$ was greater than 0.1, then the measured AOD at that wavelength was rejected. This was done to screen out AOD measurements that did not resemble an Angstrom power law. The aerosol optical depths that survived this filter were then subjected to level two of the filter. It should be noted that a given measurement consists of two series of readings, $E(\lambda)$, for each of the nine channels. This was

done to ensure that the atmosphere was stable during the measurement, as the optical depth should not change appreciably during a span of five minutes (the approximate time for one measurement). The level two filter examined the difference between the first and second measured aerosol optical depths. If the magnitude of the difference was greater than 0.03, then that channel was rejected. If only one of the two dual readings survived the level one filter, then the level two filter was not performed. Finally, the level three filter determines if at least six of the seven channels (one and nine are excluded) remain, and channels two and eight are among them. If this was true then this measurement was considered usable, else the entire measurement was discarded. The tolerance settings in the filter were the result of a trade off between eliminating questionable data, and retaining enough of the data set to analyze. This filter process ensures that the atmosphere is fairly stable, the AOD roughly resembles an Angstrom power law formula, and there are enough remaining aerosol optical depths to accurately perform a fit to the Angstrom power law (for the wavelength range, 412.2 nm to 861.8 nm only). The AOD was then calculated for the surviving measurements, and used to generate Angstrom parameters from equation 3. These surviving measurements were recorded as the optical properties for that sample.

3b. SHADOWBAND DATA FILTERING PROCEDURE

The shadowbands record data throughout the day, as opposed to the sunphotometer's singular morning and afternoon measurements. Therefore, another method of filtering out bad data was employed. The filtering procedure used for the shadowband data was based on the Sliding Window Optical Depth Procedure (SWODP) [*Jim Schlemmer, personal correspondence*] developed at the Atmospheric Sciences Research Center at the State University of New York, Albany.

The University of Miami SWODP (MSWODP) used the aerosol optical depths for each sampled measurement by the shadowband. The MSWODP then analyzed one day at a time, starting with the first measurement sample. The term, "sliding window," originated because the

MSWODP analyzed a twenty minute “window” of data to determine if the window contained usable data. Three filtering levels were then applied to the resulting AOD window by the MSWODP. The first filter performed a linear least squares fit to the AOD, and then calculated the individual AOD deviations from the fit. If all of the aerosol optical depths were within 0.01 of the linear fit then the MSWODP continued on to the next filter level for that window. If the first filter test failed then the MSWODP slid the window ahead one sample measurement and applied the filter again to the new window. If the filter one test was successful then the MSWODP applied filter two. This filter level determined the mean AOD for that window. If the mean AOD was less than 1.0 then the MSWODP recorded the mean AOD and corresponding Angstrom exponent for that window. If the mean AOD was greater than or equal to 1.0 then the entire window was rejected, and no data was recorded for that window of time. Regardless of the outcome of the filter two check, the MSWODP then slid the window ahead by twenty minutes to the corresponding sample measurement, and the process was started over again from the level one filter. The MSWODP output twenty minute averages of the AOD, and the corresponding Angstrom parameters from equation 3, for each day in the data set. Each twenty minute window of data output by the MSWODP contained aerosol optical depths that did not vary too wildly and that had AOD values reasonable for atmospheric aerosol, not clouds. The surviving measurements were recorded as the optical properties for the time of day falling at the center of the window.

3c. COMPARISON OF UNCORRECTED AND ERROR CORRECTED RESULTS

The spectral variation of the aerosol optical depths for each channel of each sunphotometer and shadowband are shown in Figs. 3a, 3b, and 3c. Each figure displays the entire data set’s uncorrected and error corrected AOD results for the sunphotometers and shadowbands.

The uncorrected sunphotometer results are not much different from the error corrected results, indicating that the data was not changed significantly by the error correction procedure. However, an improvement to the Angstrom power law fit was obtained using the error corrected

sunphotometer results. The average chi-squared data fitting parameter was reduced for each data set, indicating a better power law fit. The Miami chi-squared data fitting parameter was 0.086 for the uncorrected results and 0.034 for the error corrected results. The Bermuda uncorrected and error corrected chi-squared parameters were 0.065 and 0.012 respectively. Finally, the Barbados uncorrected and error corrected chi-squared parameters were 0.744 and 0.058. The sunphotometer error correction procedure assumes that the true AOD follows the Angstrom power law. Furthermore, the sunphotometer data filter explicitly screened out days (for both uncorrected and error corrected results) that did not accurately fit the Angstrom power law. For these two reasons, a small improvement in the fits to the Angstrom power law between uncorrected and error corrected results was expected.

There were significant differences between the uncorrected and error corrected results for certain channels of each shadowband. However, all of the error corrected changes also resulted in a better average Angstrom power law fit. In particular, the clear bias in channel five of the Miami shadowband was removed after using the shadowband error correction procedure. The Miami chi-squared data fitting parameter was 0.521 for the uncorrected results and 0.122 for the error corrected results. The Bermuda uncorrected and error corrected chi-squared parameters were 0.300 and 0.131 respectively. Finally, the Barbados uncorrected and error corrected chi-squared parameters were 0.071 and 0.059. The shadowband error correction procedure and the shadowband data filter did not assume any particular spectral form of the AOD. However, results obtained using the error corrected results more accurately portrayed a power law fit compared to the uncorrected results.

Level one of the sunphotometer data filter determined the deviation of the measured AOD from the Angstrom power law. Turning off levels two and three of the sunphotometer data filter allowed the percentage of measurements rejected by only level one to be determined. The level one sunphotometer data filter rejected 3% of the Barbados measurements and 7% of the Miami and Bermuda measurements. Therefore, at all three locations, over 90% of the sunphotometer AOD measurements resembled an Angstrom power law. Also, there were significant improvements in

the Angstrom power law fits using the error corrected shadowband results compared to using the uncorrected shadowband data. This improvement indicates that the majority of shadowband AOD measurements also resembled an Angstrom power law, particularly since no spectral dependence of the AOD was assumed but the error corrected data more accurately fit the Angstrom power law. As a result of this analysis, the majority of the aerosol optical depths measured over Miami, Bermuda, and Barbados were found to accurately depict an Angstrom power law in the wavelength range 400 nm to 860 nm.

4. FINAL RESULTS AND CONCLUSION

The sunphotometer and shadowband results, obtained using the filtering procedures of the previous section, were merged together and monthly mean values of both the AOD at 500 nm and the corresponding Angstrom exponent were recorded. This was accomplished for each measurement site. The monthly mean values for Miami, Bermuda, and Barbados are depicted graphically in Figs. 4a, 4b, and 4c. Table 3 contains the monthly mean values mentioned above and the Angstrom scale factor, β , for each measurement site, as well as the total mean values.

Seasonal variability of the AOD existed for each site. Peaks in the Miami AOD occurred primarily during the May to June periods. The Barbados AOD results also indicated clear peaks from the May to August periods. The Bermuda AOD results were not as obvious, however, elevated AOD values were found during the April to June periods. Each site also has shown minimum AOD levels during the winter months. This pattern of seasonal variability in the AOD has been documented previously [Malm *et. al.*, 1994; Smirnov *et. al.*, 1995; Husar *et. al.*, Submitted *JGR* 1996]. Seasonal trends in the Angstrom exponents were not easy to deduce from the monthly mean values as the exponents vary widely from day to day, due not only to changing aerosol types but also to changing meteorological conditions. However, the Miami and Bermuda exponents did show a tendency to drop during the summer months, relative to levels during the spring and early

fall. Barbados exponents also have shown a tendency to drop relative to surrounding months, but during April to June 1994 and the summer of 1995. These seasonal trends in the optical properties for each site are due in large part to the origin [Smirnov *et. al.*, 1995] and seasonal variability in the type and concentration of the major aerosol species found at each site [Welton *et. al.*, 1997].

The high degree to which the aerosols at each site could be characterized by the Angstrom power law was greater than expected. If there had not been a strong AOD power law dependence on average, the shadowband error correction procedure would not have correlated as well with the sunphotometer results. The spectral variation of the AOD is an important parameter in determining the atmospheric path radiance, used primarily in remote sensing applications. Kaufman [1993] has shown that the path radiance over land can be derived more accurately using aerosol optical depths derived from an average Angstrom exponent rather than individual measurement exponents, except for conditions dominated by dust. The tendency of our maritime aerosol optical depth results to fit the Angstrom power law on average indicates that it may be possible to use the same condition to generate the path radiance over the ocean. Due to the sharp difference between the spectral dependence of dust dominated AOD and that of other maritime aerosols [Binenko *et. al.*, 1993; Welton *et. al.*, 1997], it is also possible that the same exclusion conditions apply to the calculation of the maritime path radiance during dusty periods.

Further analysis of the aerosol optical depth and Angstrom parameter results must take into account individual aerosol types and concentrations, as well as seasonal trends in the aerosol's transport from their points of origin. Analysis of this type may be added to the results contained in this paper to produce a characteristic description of the aerosol over a particular site. Long term data records of these aerosol properties over several different sites will also help track trends in global climate change. The measurement programs described in this paper will continue until the end of the AEROCE program (DATE??) in order to extend the data sets presented above. In addition, two more shadowbands have been installed in Tenerife, located in the Canary Islands. One is located at the mountain top weather station at Izana, a long time AEROCE site, and the other is located in La Laguna, at sea level. The Tenerife shadowbands will produce optical data close to

the primary source of north Atlantic ocean dust, the Saharan desert [*Prospero, 1995*]. Also, they will allow the comparison of optical properties taken below the aerosol boundary layer to those taken above it, as the boundary layer often lies between Izana and sea level [reference]. Finally, specific correlations between aerosol types, concentrations and optical properties are the subject of another paper by the authors [*Welton et. al., 1997*].

REFERENCES

- Angstrom, A., The Parameters of Atmospheric Turbidity, *Tellus*, 16, 64-75, 1964.
- Binenko, V.I., and H. Harshvardhan, Aerosol Effects in Radiation Transfer, Chapter in *Aerosol Effects on Climate*, Univ. of Arizona Press, Tucson, Arizona, 1993.
- Charlson, R.J., S.E. Schwartz, J.M. Hales, R.D. Cess, J.A. Coakley Jr., J.E. Hansen, D.J. Hofmann, Climate Forcing by Anthropogenic Aerosols, *Science*, 255, 423-430, 1992.
- Hansen, J.E., and L.D. Travis, Light Scattering in Planetary Atmospheres, *Space Sci. Reviews*, 16, 527-610, 1974.
- Harrison, L., J. Michalsky, and J. Berndt, The Automated Multi-Filter Rotating Shadow-band Radiometer: An Instrument for Optical Depth and Radiation Measurements, *Appl. Optics*, 33, 5118-5125, 1994.
- Harrison, L., and J. Michalsky, Objective Algorithms for the Retrieval of Optical Depths From Ground-Based Measurements, *Appl. Optics*, 33, 5126-5132, 1994.
- Husar, R.B., L. Stowe, and J. Prospero, Satellite Sensing of Tropospheric Aerosols Over the Oceans with NOAA AVHRR, *Submitted to J. Geophys. Res.*, 1996.
- Kasten, F., and A.T. Young, Revised optical air mass tables and approximation formula, *Appl. Optics*, 28, 4735-4738, 1989.
- Kaufman, Y.J., Aerosol Optical Thickness and Atmospheric Path Radiance, *J. Geophys. Res.*, 98, 2677-2692, 1993.
- King, M., D. Byrne, J. Reagan, and B. Herman, Spectral Variation of Optical Depth at Tucson Arizona Between August 1975 and December 1977, *J. Appl. Meteorol.*, 19, 16,639-16,650, 1980.
- Klenk, K., P. Bhartia, E. Hilsenrath, and A. Fleig, Standard Ozone Profiles From Balloon and Satellite Data Sets, *J. Clim. Appl. Meteorol.*, 22, 2012-2022, 1983.
- Malm, W.C., J. Sisler, D. Huffman, R. Eldred, and T. Cahill, Spatial and Seasonal Trends in Particle Concentration and Optical Extinction in the United States, *J. Geophys. Res.*, 99, 1347-1370, 1994.
- Prospero, J.M., Saharan Dust Transport Over The North Atlantic Ocean and Mediterranean, Chapter in *The Impact of Desert Dust From Northern Africa Across the Mediterranean*, Kluwer Academic Publishers, Oristano, Sardinia, 1995.
- Shaw, G., Aerosols at Mauna Loa: Optical Properties, *J. Atmos. Sci.*, 36, 862-869, 1979.
- Shaw, G., Sun Photometry, *Bulletin American Meteorol. Soc.*, 64, 4-9, 1983.
- Smirnov, A., Y. Villevalde, N. O'Neill, A. Royer, and A. Tarussov, Aerosol Optical Depth Over the Oceans: Analysis in Terms of Synoptic Air Mass Types, *J. Geophys. Res.*, 100, 16639-16650, 1995.
- Van de Hulst, H. C., *Light Scattering by Small Particles*, Dover Publications Inc., New York, NY, 1981.
- Villevalde, Y.V., A.V. Smirnov, N.T. O'Neill, S.P. Smyshlyaev, and V.V. Yakovlev, Measurement of aerosol optical depth in the Pacific Ocean and the North Atlantic, *J. Geophys. Res.*, 99, 20983-20988, 1994.
- Welton, E.J., K.J. Voss, and J.M. Prospero, Radiative Characteristics of Specific Types and Concentrations of Maritime Aerosols, *Submitted to J. Geophys. Res.*, 1997.
- Gordon, H.R., Ocean Color Correction reference.....
- AEROCE Reference.....
- Personal Correspondence: Background AOD Dependence on 1/airmass.....
- Personal Correspondence: Jim Schlemmer, Sliding Window Reference.....
- Reference for Tenerife boundary layer, etc.....

Table 1. Instrumentation Location Information

Location	Latitude	Longitude	Altitude	Sunphotometer	Shadowband
				Time Period	Time Period
Miami, Fl	25.75	80.2	Sea Level	Aug93 to Nov94	May94 to Dec95
Barbados	13.18	59.43	Sea Level	Aug93 to Sep94	Jul94 to Dec95
Bermuda	32.38	64.70	Sea Level	Aug93 to Nov94	Nov94 to Dec95

Table 2. Instrument Channel Numbers and Filter Wavelengths (nm)

Channel Number	Sunphotometer Wavelength (nm)	Shadowband Wavelength (nm)
1	380.2	Broadband
2	412.2	410
3	440.5	500
4	501.8	610
5	551.2	665
6	675.2	860
7	777.9	940
8	861.8	-
9	1025.9	-

TABLE 3a: Miami Monthly Mean Aerosol Optical Depths and Angstrom Parameters (Aug93 to Dec95)

Number of samples

Month-Year	$\bar{\tau}_{a_{500}}$	σ_{τ}	$\bar{\beta}$	σ_{β}	$\bar{\alpha}$	σ_{α}
Aug-93	-	-	-	-	-	-
Sep-93	0.114	0.024	0.070	0.022	0.734	0.228
Oct-93	0.142	0.068	0.069	0.020	0.976	0.374
Nov-93	0.142	0.020	0.080	0.011	0.833	0.001
Dec-93	0.121	0.034	0.050	0.013	1.269	0.056
Jan-94	0.121	0.030	0.071	0.005	0.740	0.398
Feb-94	0.120	0.035	0.083	0.035	0.566	0.375
Mar-94	0.151	0.073	0.069	0.030	1.063	0.240
Apr-94	0.166	0.038	0.104	0.035	0.706	0.553
May-94	0.243	0.091	0.111	0.033	1.098	0.319
Jun-94	0.163	0.058	0.128	0.057	0.217	0.457
Jul-94	0.234	0.055	0.209	0.034	0.148	0.100
Aug-94	0.075	0.013	0.059	0.011	0.347	0.319
Sep-94	0.127	0.058	0.079	0.026	0.524	0.773
Oct-94	0.119	0.054	0.056	0.027	0.987	0.509
Nov-94	0.093	0.039	0.049	0.014	0.762	0.713
Dec-94	0.097	0.041	0.093	0.019	-0.246	0.820
Jan-95	0.091	0.032	0.059	0.017	0.443	0.579
Feb-95	0.115	0.049	0.062	0.024	0.846	0.501
Mar-95	0.118	0.020	0.065	0.010	0.768	0.284
Apr-95	0.143	0.037	0.094	0.019	0.480	0.311
May-95	0.288	0.078	0.108	0.023	1.294	0.199
Jun-95	-	-	-	-	-	-
Jul-95	0.165	0.053	0.103	0.030	0.494	0.565
Aug-95	0.148	0.077	0.100	0.043	0.347	0.557
Sep-95	-	-	-	-	-	-
Oct-95	-	-	-	-	-	-
Nov-95	-	-	-	-	-	-
Dec-95	0.099	0.032	0.045	0.016	1.110	0.565
Total	0.141	0.050	0.084	0.034	0.684	0.367

TABLE 3b: Bermuda Monthly Mean Aerosol Optical Depths and Angstrom Parameters (Aug93 to Dec95)

Number of samples

Month-Year	$\bar{\tau}_{a_{500}}$	σ_{τ}	$\bar{\beta}$	σ_{β}	$\bar{\alpha}$	σ_{α}
Aug-93	-	-	-	-	-	-
Sep-93	0.161	0.043	0.104	0.015	0.603	0.290
Oct-93	0.161	0.041	0.103	0.020	0.622	0.232
Nov-93	0.117	0.025	0.081	0.018	0.540	0.214
Dec-93	0.160	0.037	0.102	0.009	0.614	0.304
Jan-94	0.099	0.012	0.069	0.011	0.531	0.298
Feb-94	0.102	0.023	0.079	0.005	0.322	0.372
Mar-94	0.157	0.041	0.099	0.026	0.666	0.268
Apr-94	0.169	0.050	0.105	0.022	0.667	0.415
May-94	0.134	0.047	0.085	0.030	0.655	0.259
Jun-94	0.270	0.125	0.170	0.072	0.599	0.233
Jul-94	0.116	0.072	0.081	0.045	0.474	0.179
Aug-94	0.126	0.131	0.097	0.125	0.424	0.334
Sep-94	0.100	0.061	0.049	0.035	1.058	0.746
Oct-94	0.075	0.041	0.060	0.015	0.288	0.663
Nov-94	0.068	0.021	0.077	0.016	-0.209	0.351
Dec-94	0.064	0.028	0.085	0.033	-0.920	0.973
Jan-95	0.081	0.035	0.075	0.023	-0.236	0.817
Feb-95	0.104	0.027	0.059	0.025	0.697	0.616
Mar-95	0.091	0.050	0.068	0.023	0.108	0.416
Apr-95	0.172	0.077	0.095	0.034	0.818	0.187
May-95	0.168	0.057	0.088	0.030	0.851	0.318
Jun-95	0.134	0.069	0.072	0.024	0.558	0.659
Jul-95	-	-	-	-	-	-
Aug-95	-	-	-	-	-	-
Sep-95	-	-	-	-	-	-
Oct-95	-	-	-	-	-	-
Nov-95	-	-	-	-	-	-
Dec-95	-	-	-	-	-	-
Total	0.129	0.047	0.086	0.025	0.442	0.433

TABLE 3c: Barbados Monthly Mean Aerosol Optical Depths and Angstrom Parameters (Aug93 to Dec95)

Number of samples

Month-Year	$\bar{\tau}_{a_{500}}$	σ_{τ}	$\bar{\beta}$	σ_{β}	$\bar{\alpha}$	σ_{α}
Aug-93	-	-	-	-	-	-
Sep-93	-	-	-	-	-	-
Oct-93	0.078	0.033	0.059	0.029	0.442	0.166
Nov-93	0.072	0.019	0.055	0.021	0.483	0.256
Dec-93	0.064	0.006	0.051	0.015	0.360	0.322
Jan-94	0.084	0.029	0.071	0.022	0.262	0.180
Feb-94	0.129	0.057	0.097	0.055	0.508	0.446
Mar-94	0.078	0.058	0.064	0.056	0.605	0.674
Apr-94	0.184	0.157	0.167	0.156	0.275	0.245
May-94	0.201	0.151	0.167	0.102	0.256	0.245
Jun-94	0.247	0.095	0.224	0.084	0.148	0.139
Jul-94	0.362	0.128	0.267	0.111	0.504	0.225
Aug-94	0.210	0.067	0.132	0.055	0.731	0.211
Sep-94	0.169	0.090	0.118	0.076	0.640	0.287
Oct-94	-	-	-	-	-	-
Nov-94	-	-	-	-	-	-
Dec-94	-	-	-	-	-	-
Jan-95	-	-	-	-	-	-
Feb-95	-	-	-	-	-	-
Mar-95	-	-	-	-	-	-
Apr-95	-	-	-	-	-	-
May-95	-	-	-	-	-	-
Jun-95	0.257	0.107	0.260	0.108	0.014	0.059
Jul-95	0.144	0.060	0.147	0.063	0.047	0.187
Aug-95	0.200	-	0.176	-	0.138	-
Sep-95	-	-	-	-	-	-
Oct-95	-	-	-	-	-	-
Nov-95	-	-	-	-	-	-
Dec-95	-	-	-	-	-	-
Total	0.165	0.085	0.137	0.073	0.361	0.220

Figure 1a.

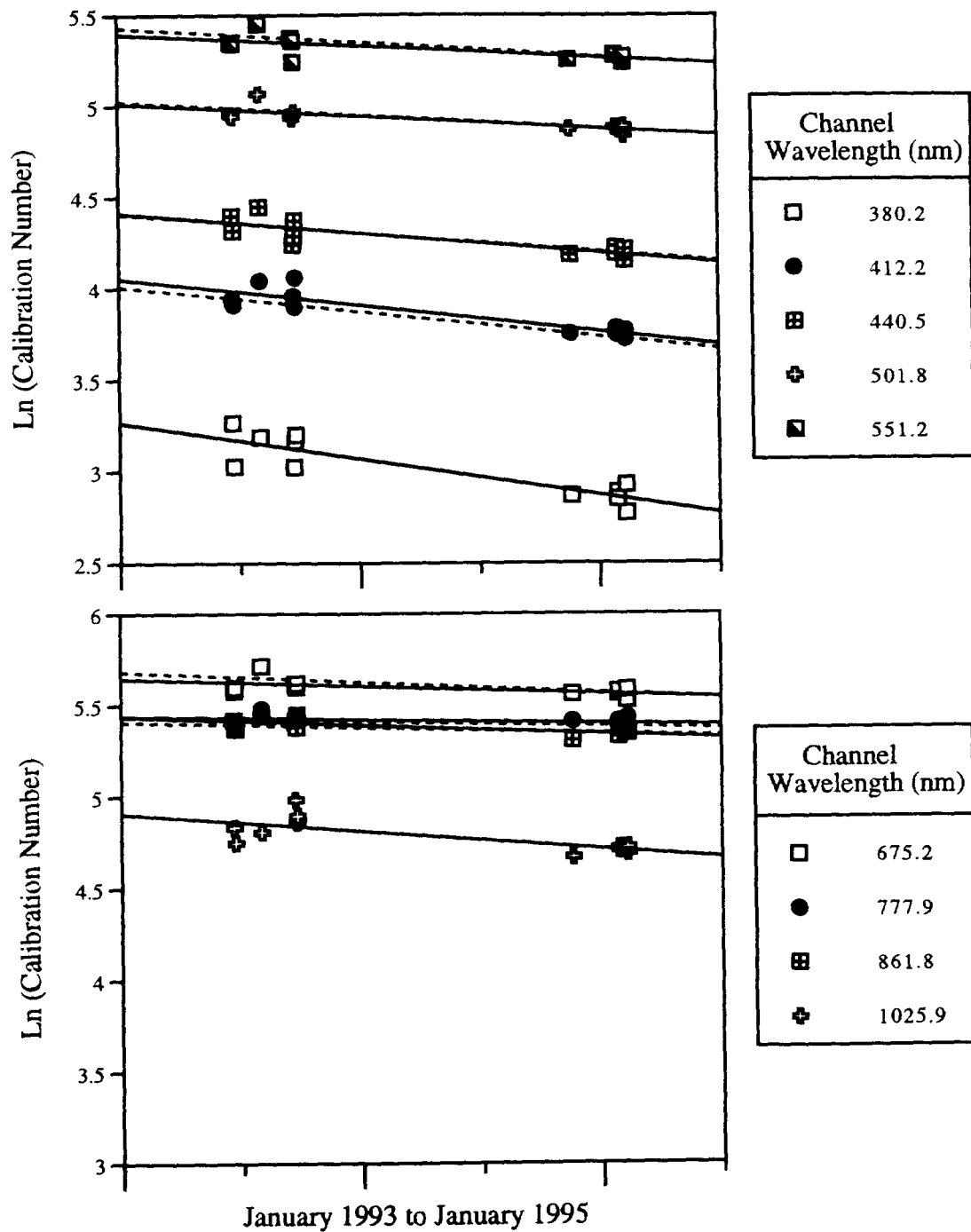


Figure 1a. Calibration history for the Miami sunphotometer. The solid line is the exponential fit to the Langley and cross-calibrations. The dotted line is the exponential fit to the error corrected Langley and cross-calibrations.

Figure 1b.

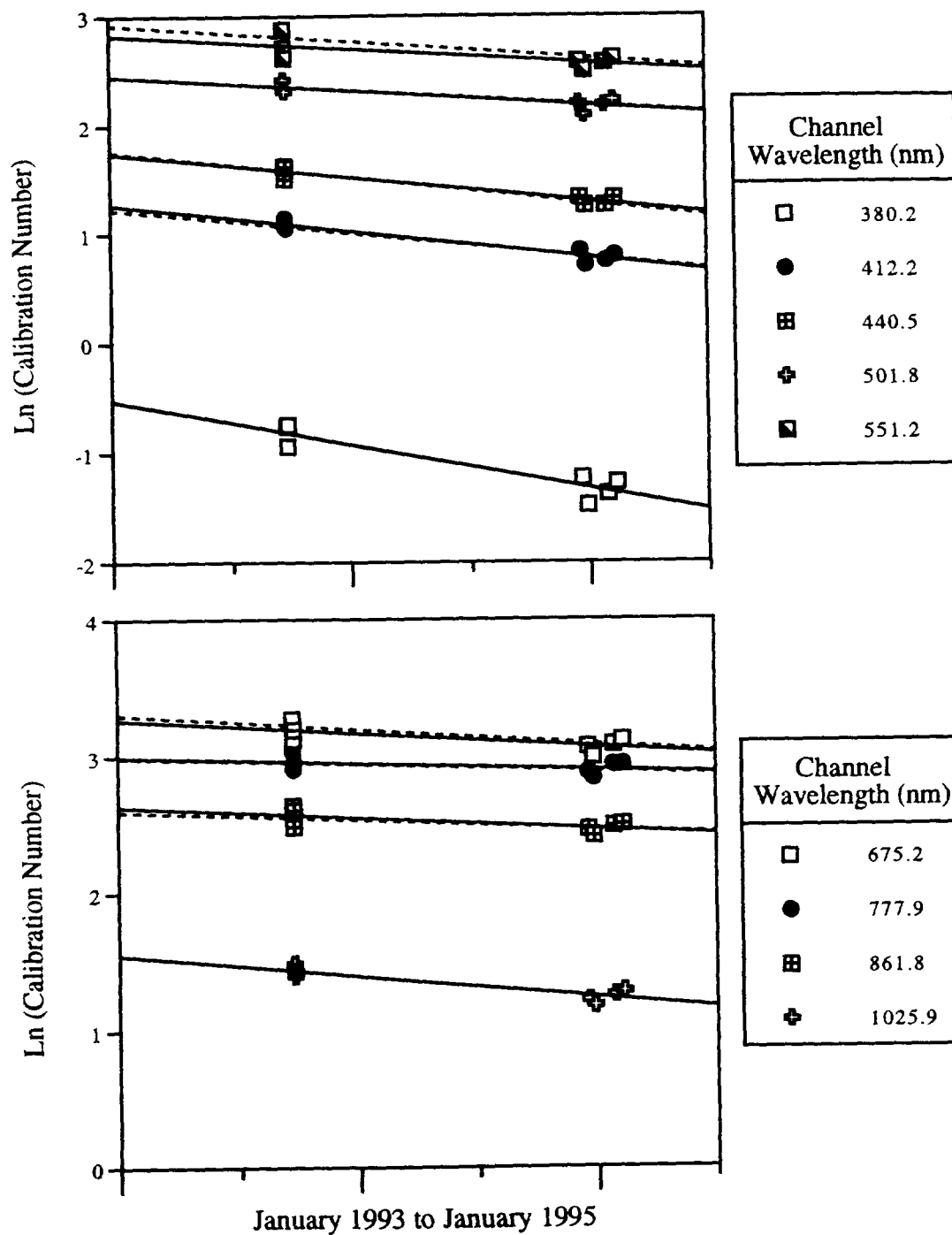


Figure 1b. Calibration history for the Barbados sunphotometer. The solid line is the exponential fit to the Langley and cross-calibrations. The dotted line is the exponential fit to the error corrected Langley and cross-calibrations.

Figure 1c.

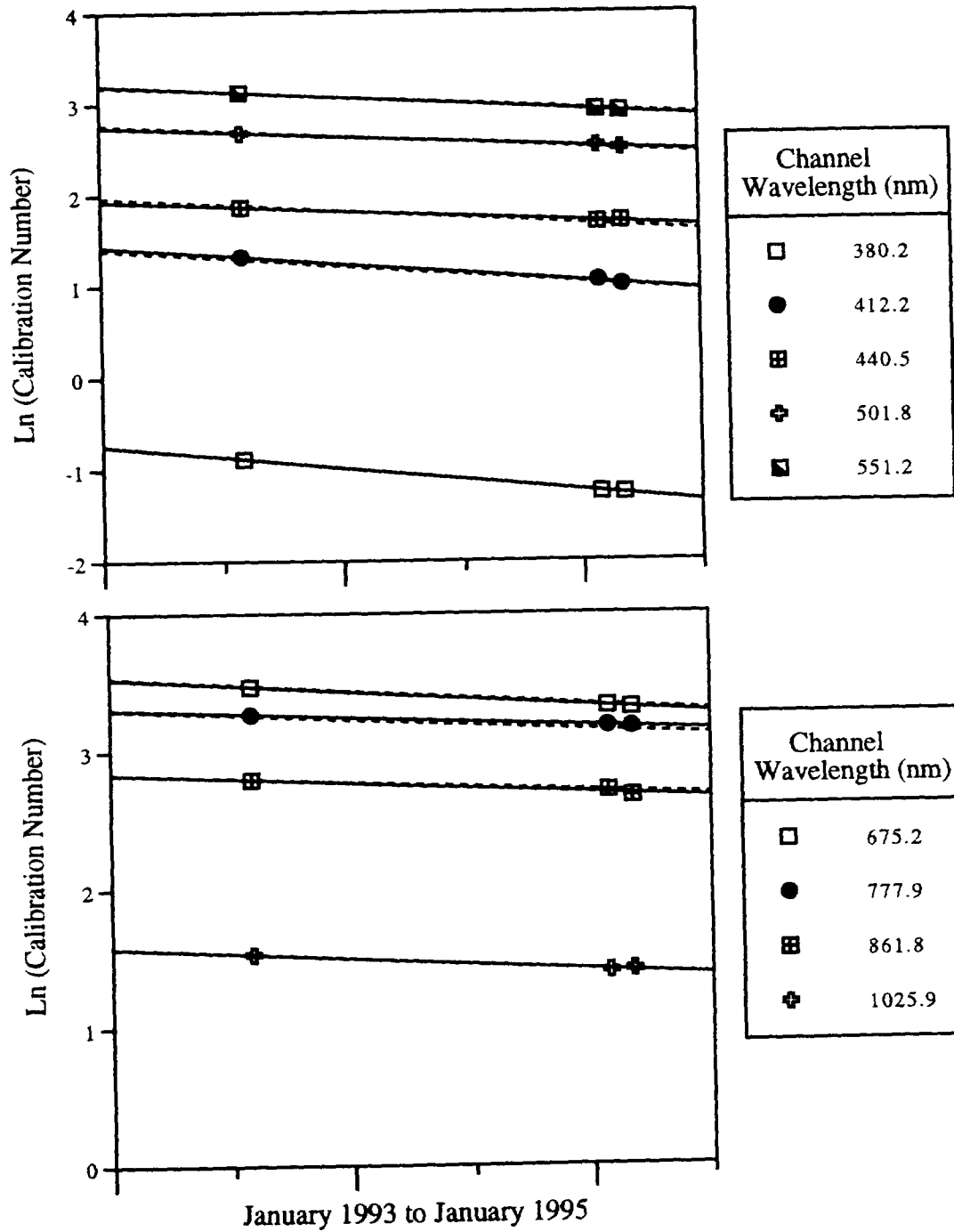


Figure 1c. Calibration history for the Bermuda sunphotometer. The solid line is the exponential fit to the Langley and cross-calibrations. The dotted line is the exponential fit to the error corrected Langley and cross-calibrations.

Figure 2a

Miami Shadowband Calibration History: May94 to Dec95

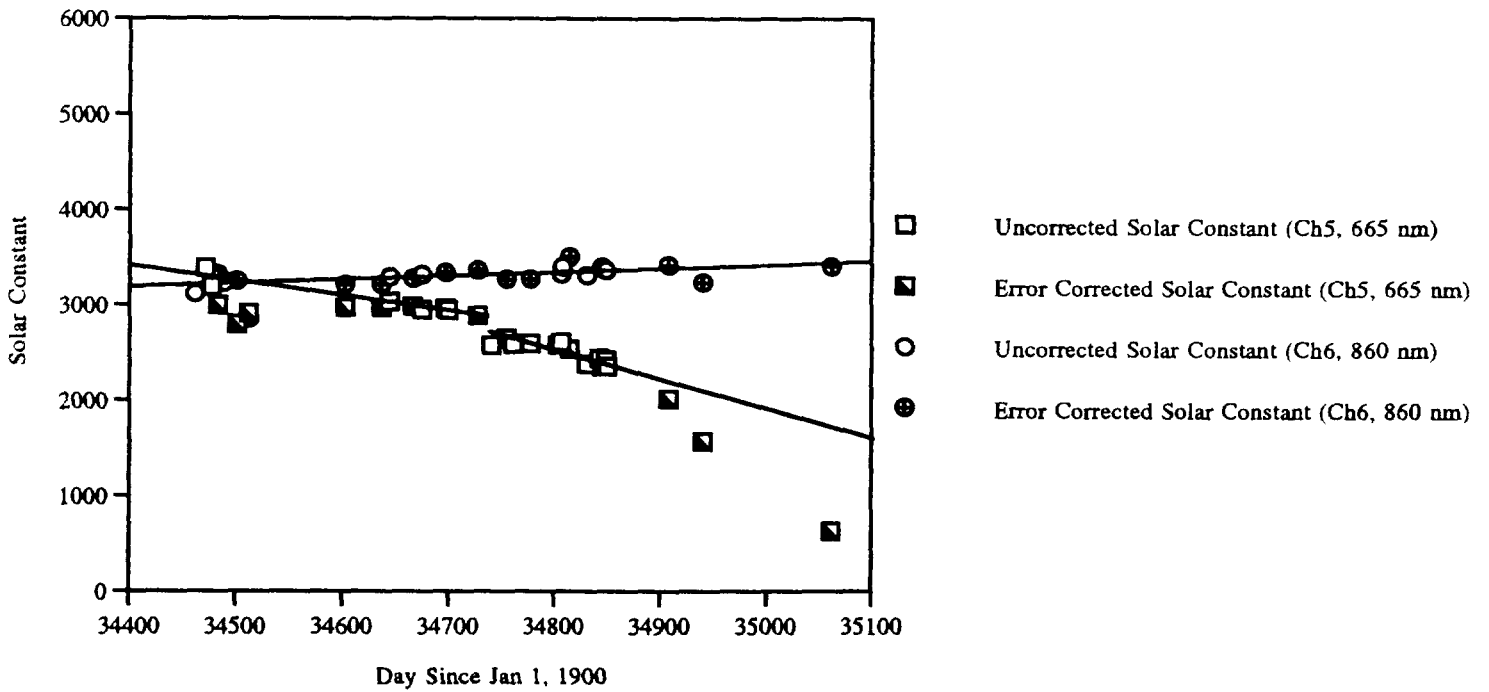
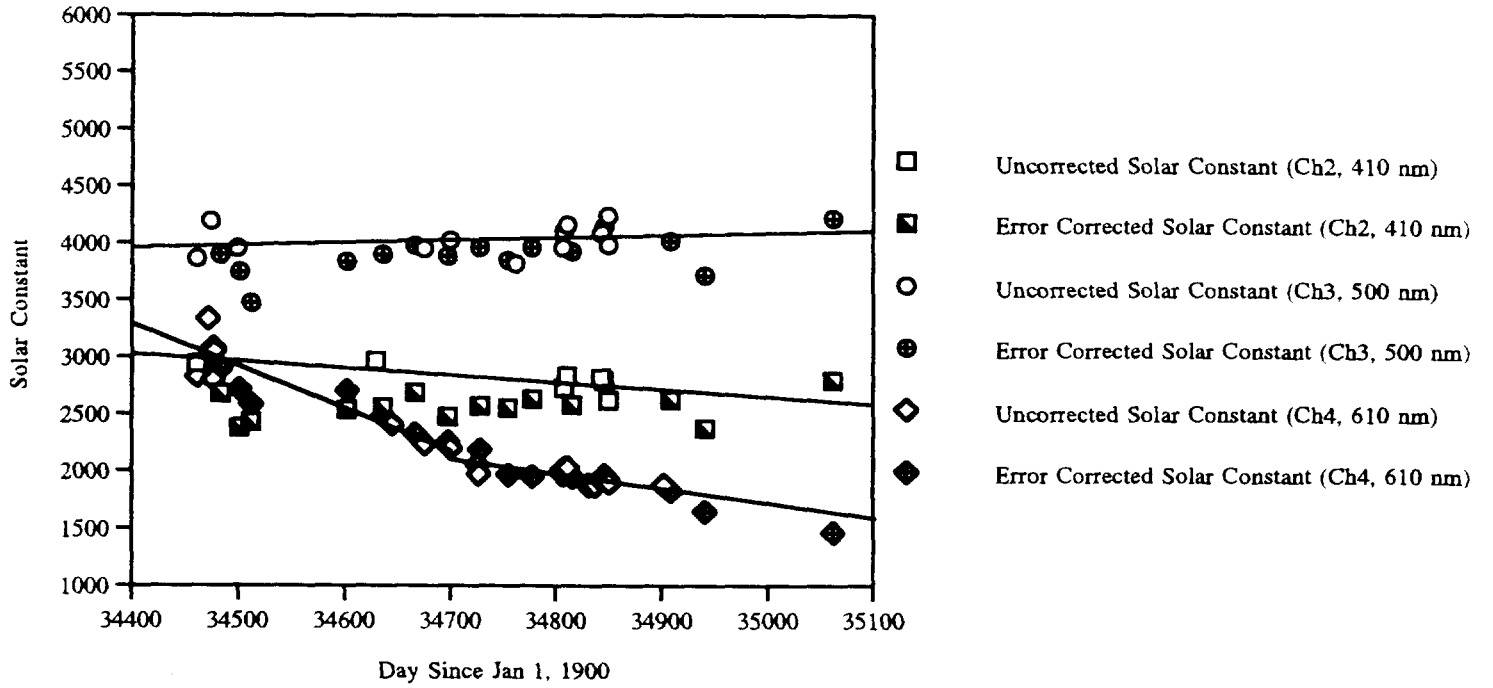


Figure 2b

Bermuda Shadowband Calibration History: May94 to Dec95

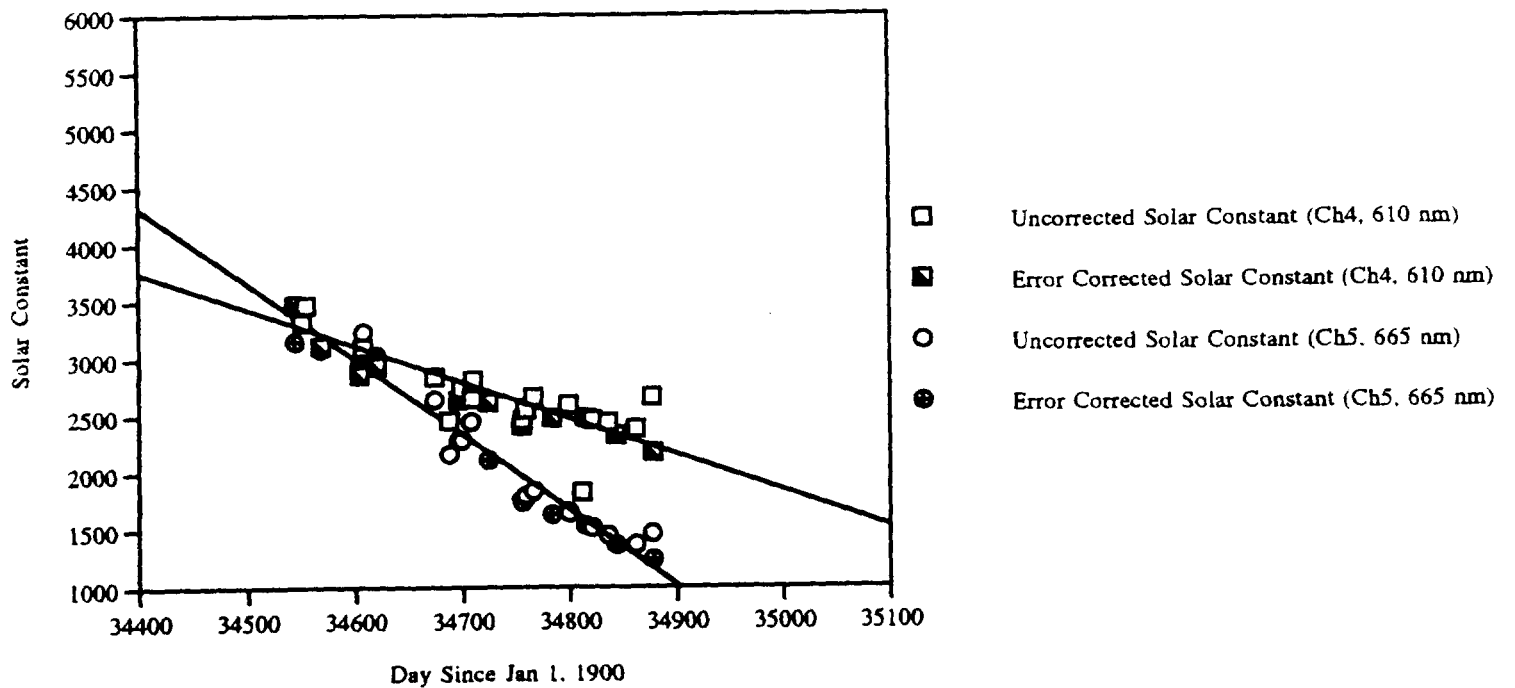
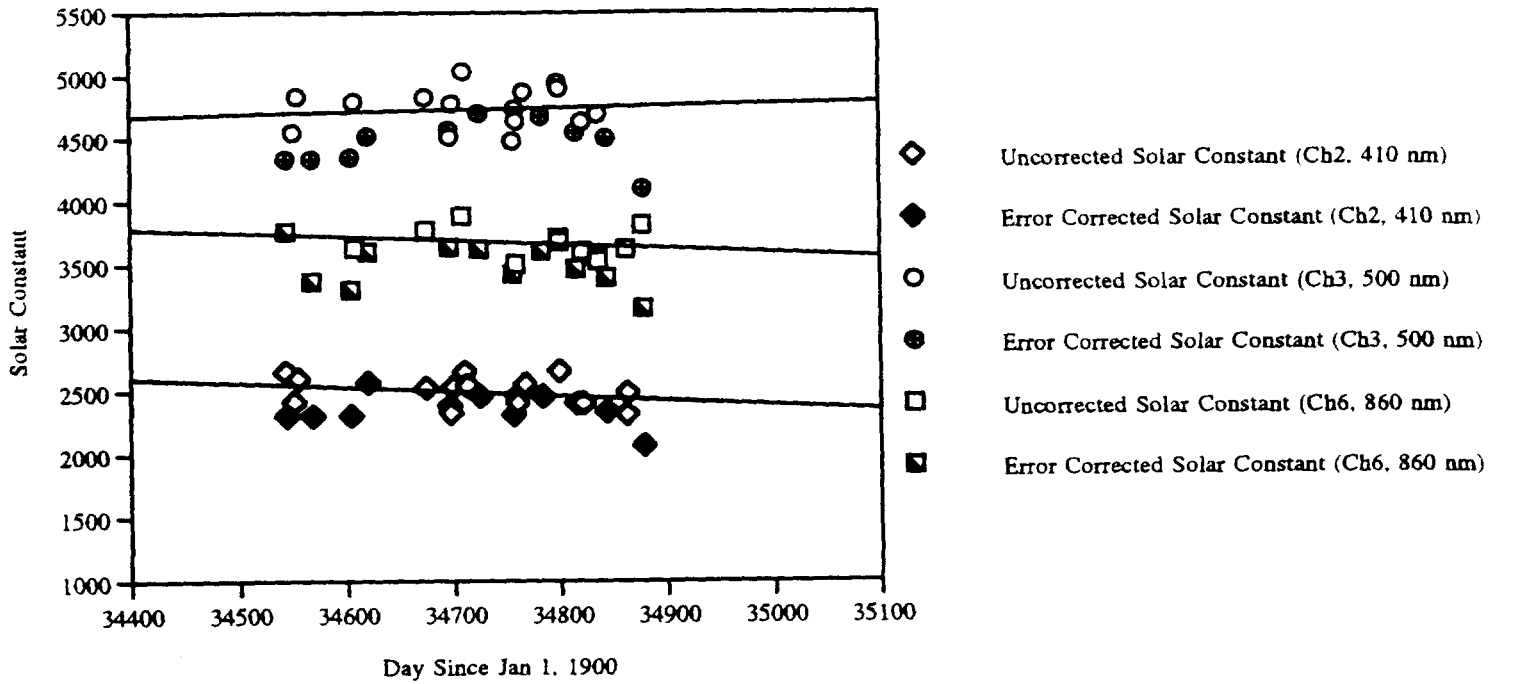


Figure 2c

Barbados Shadowband Calibration History: Jun95 to Aug95

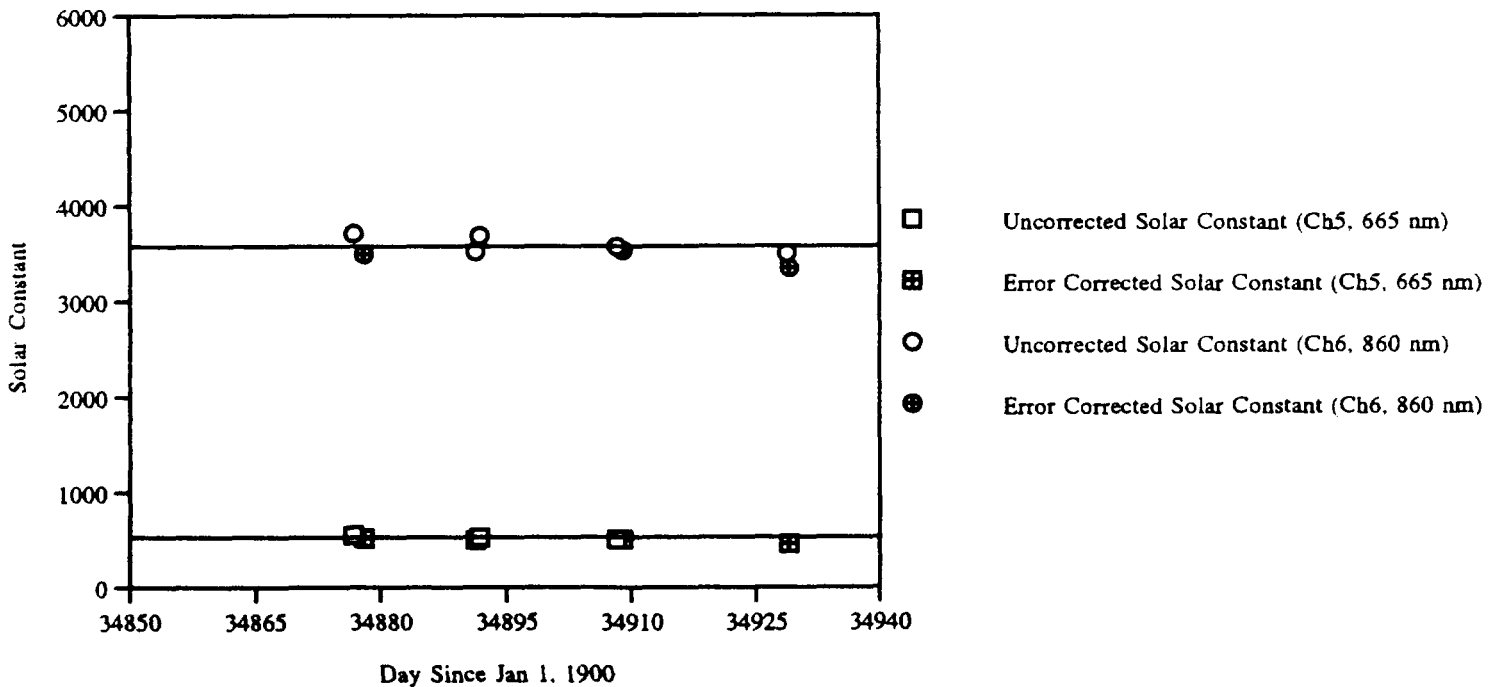
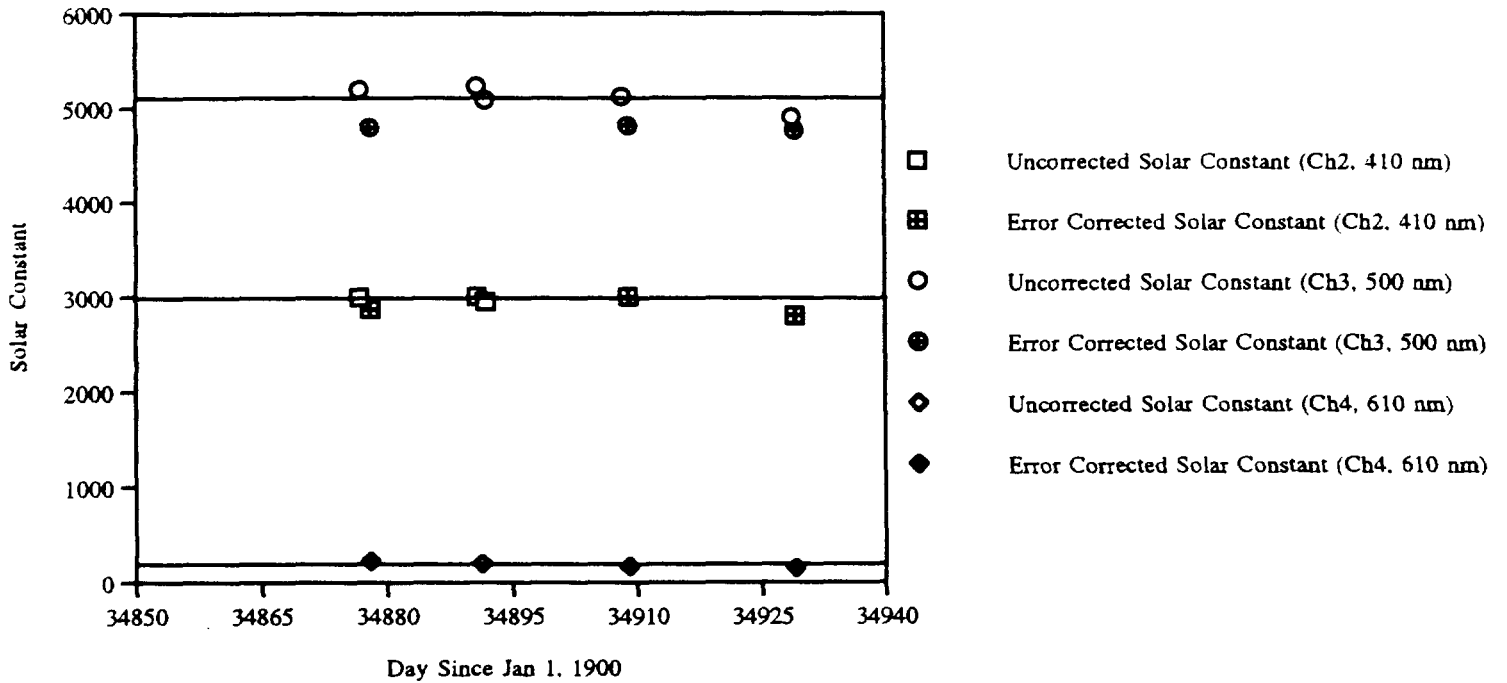
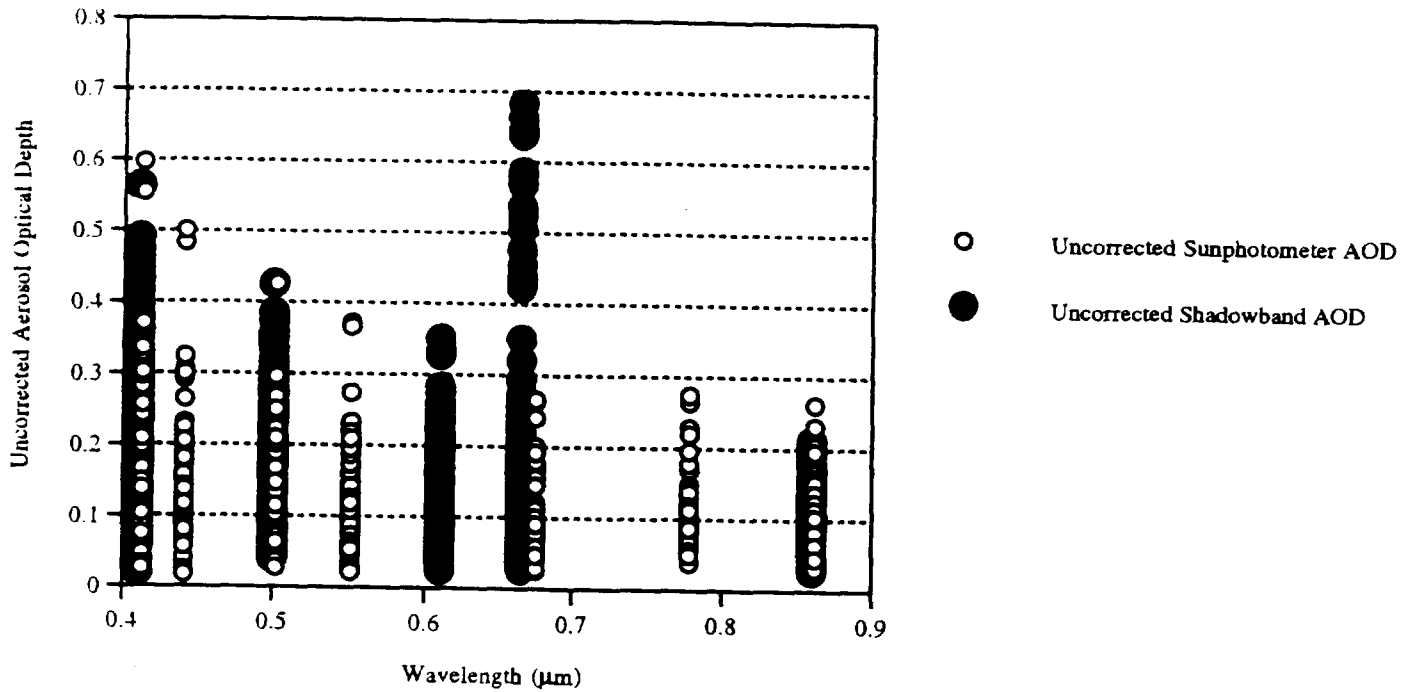


Figure 3a

Miami AOD vs. Wavelength: Uncorrected Results (Aug93 to Dec95)



Miami AOD vs. Wavelength: Error Corrected Results (Aug93 to Dec95)

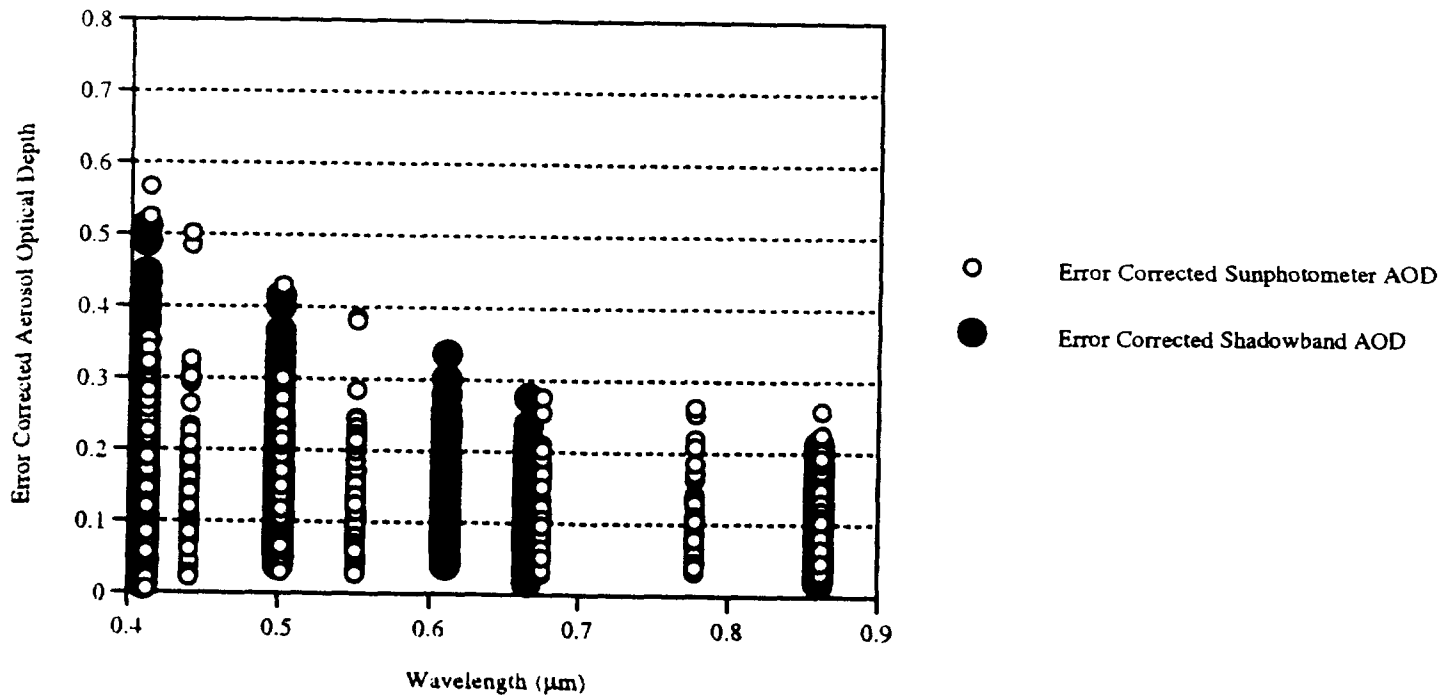
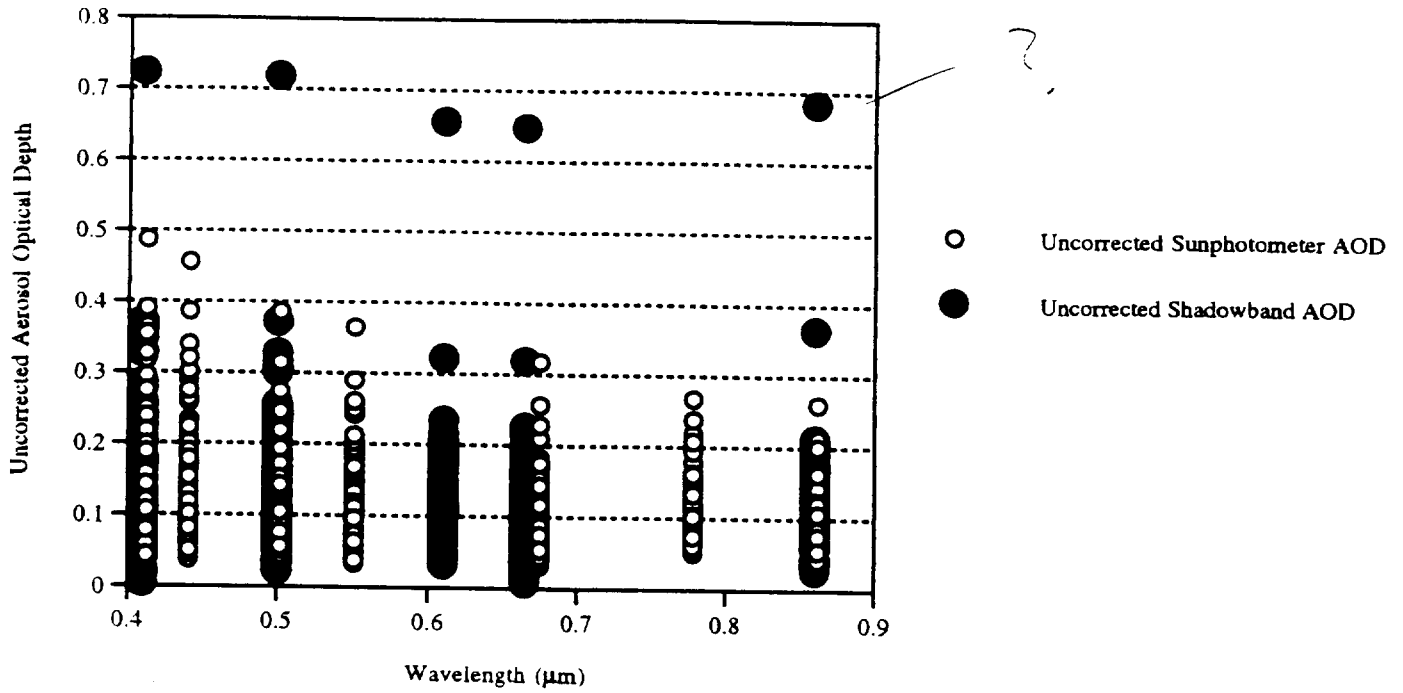


Figure 3b

Bermuda AOD vs. Wavelength: Uncorrected Results (Aug93 to Dec95)



Bermuda AOD vs. Wavelength: Error Corrected Results (Aug93 to Dec95)

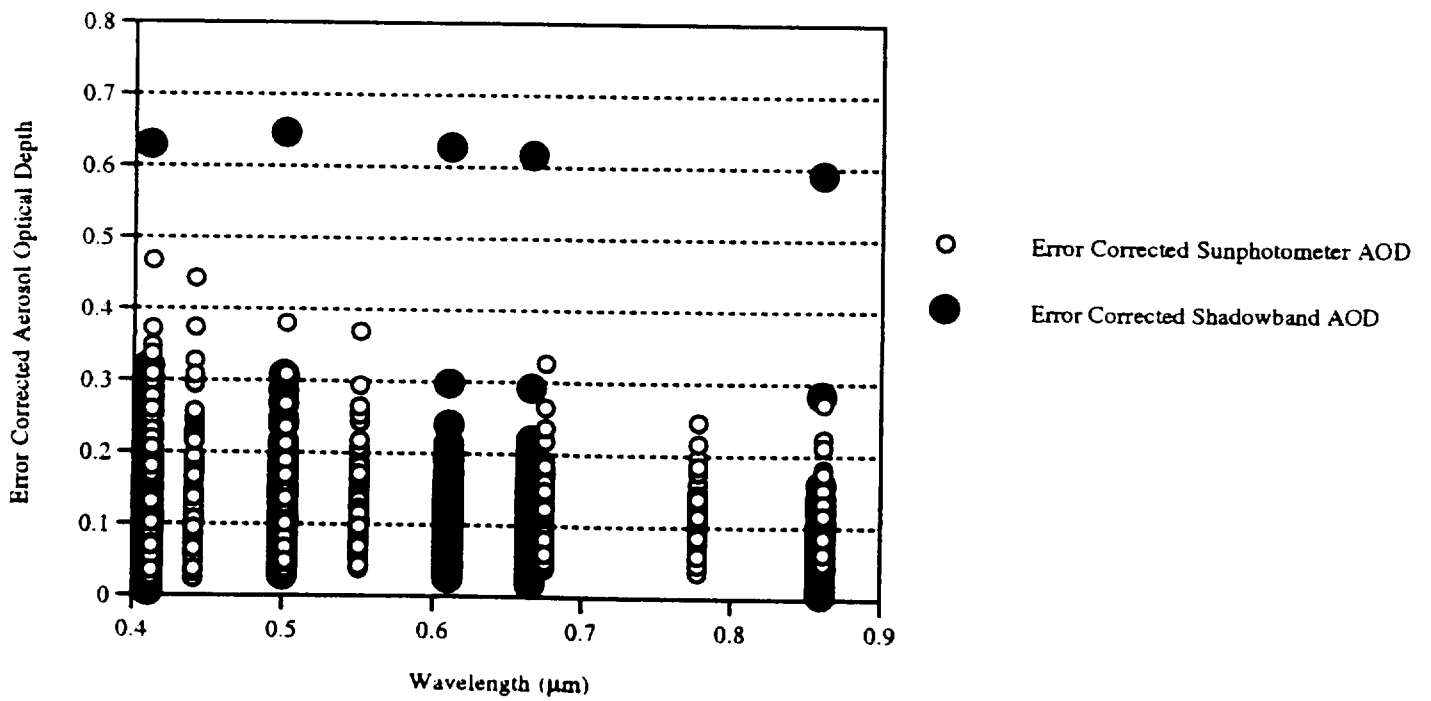
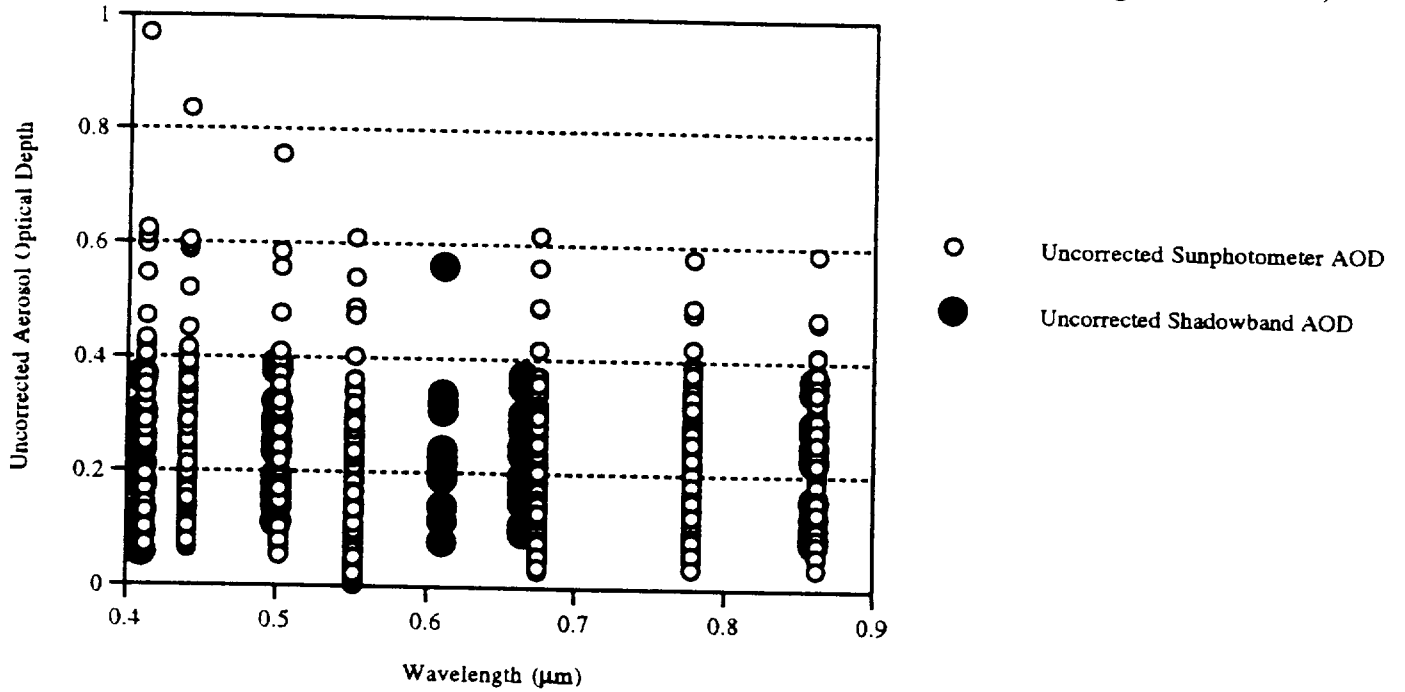


Figure 3c

Barbados AOD vs. Wavelength: Uncorrected Results (Aug93 to Dec95)



Barbados AOD vs. Wavelength: Error Corrected Results (Aug93 to Dec95)

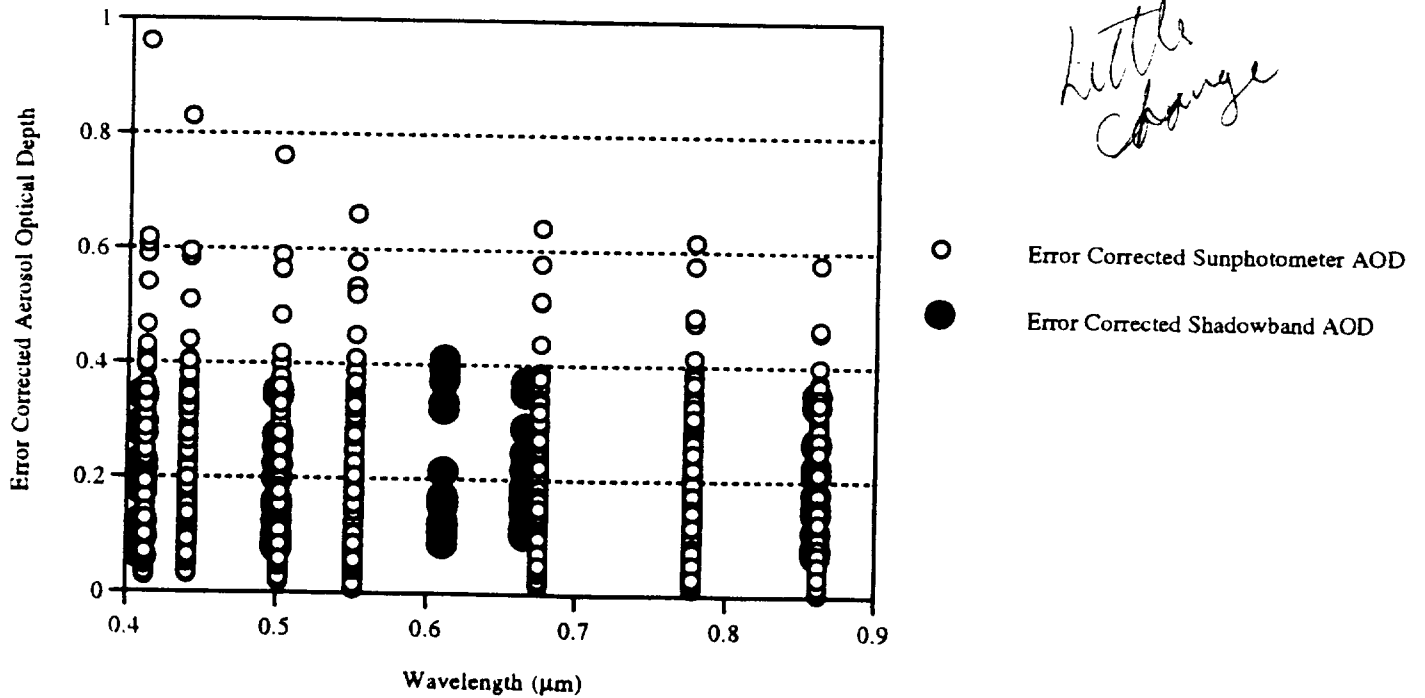


Figure 4a

Miami AOD and Angstrom Exponent Monthly Averages: Aug93 to Dec95

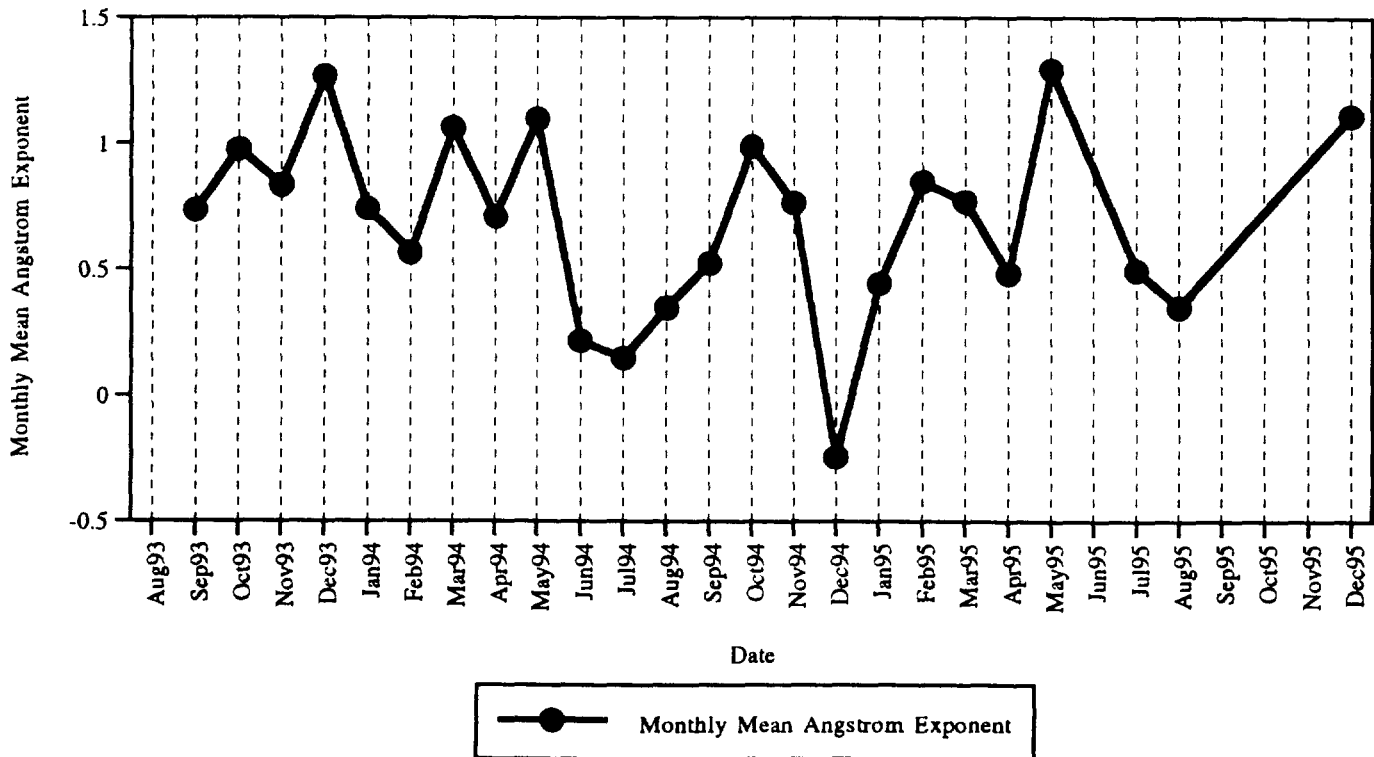
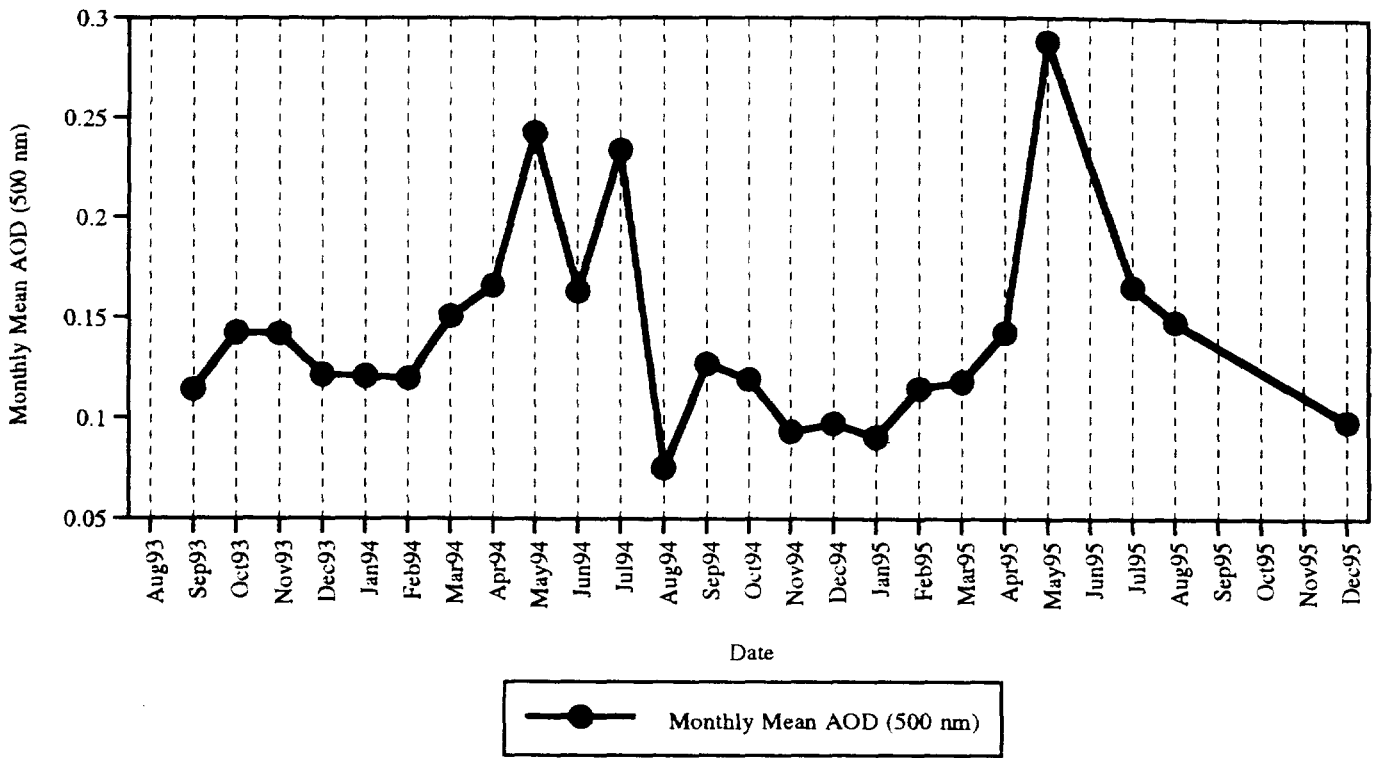


Figure 4b

Bermuda AOD and Angstrom Exponent Monthly Averages: Aug93 to Dec95

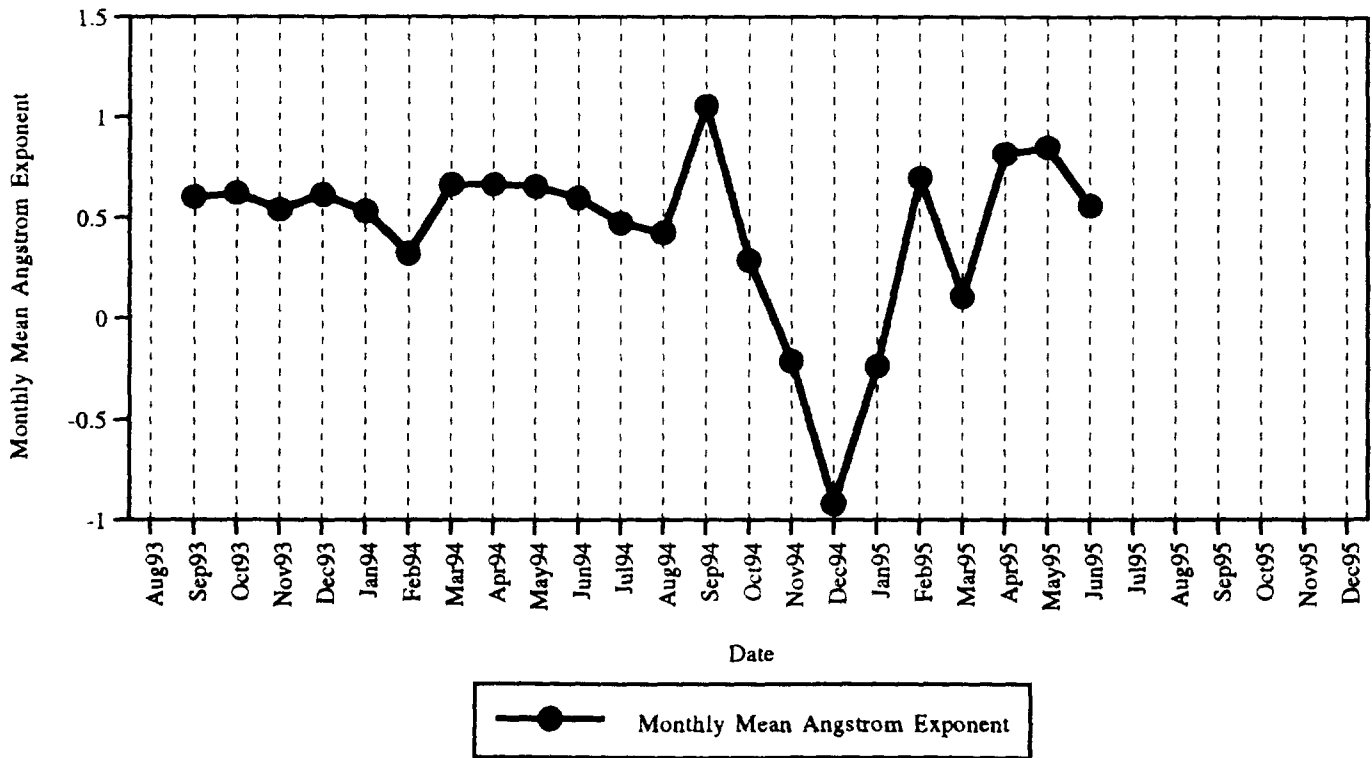
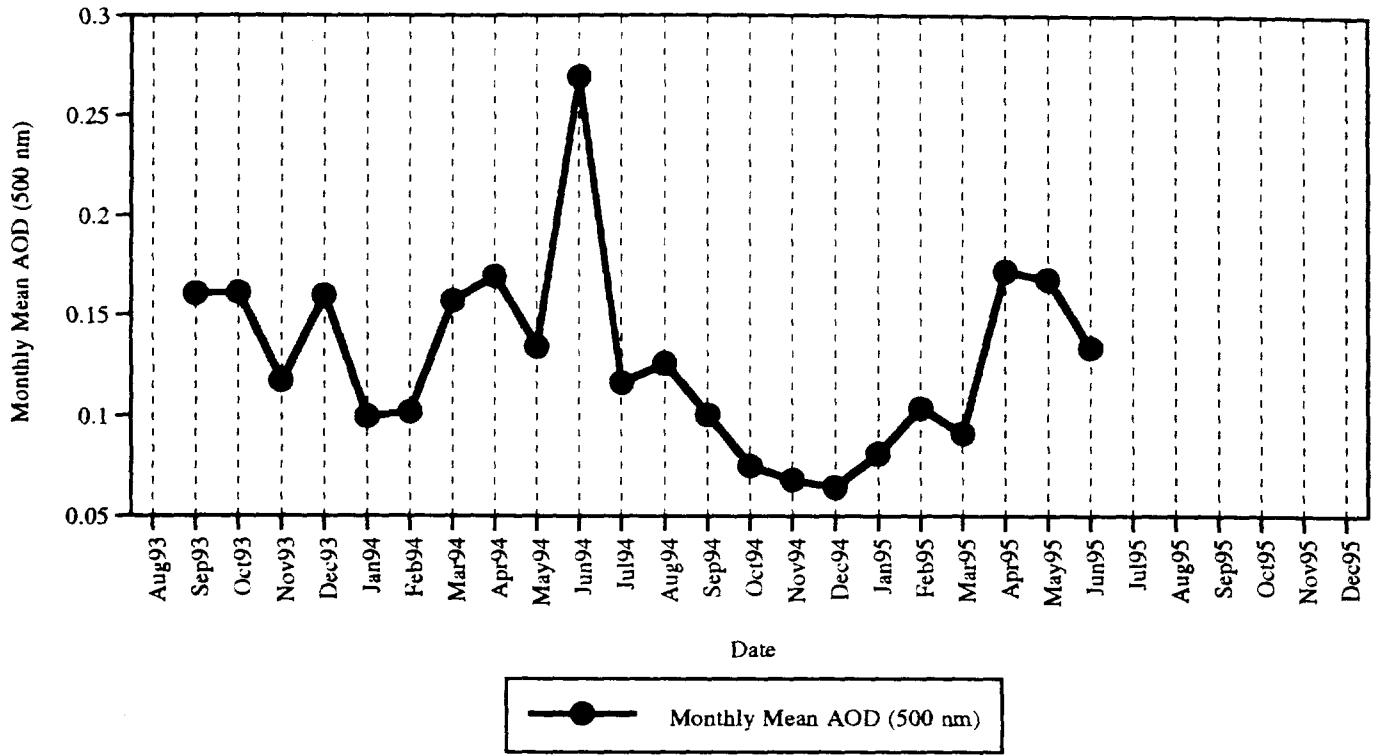


Figure 4c

Barbados AOD and Angstrom Exponent Monthly Averages: Aug93 to Dec95

